

# Hybrid improved empirical mode decomposition and BP neural network model for the prediction of sea surface temperature

Zhiyuan Wu<sup>a,b,c</sup>, Changbo Jiang<sup>a,c,\*</sup>, Mack Conde<sup>d</sup>, Bin Deng<sup>a,c</sup>, Jie Chen<sup>a,c</sup>

a. School of Hydraulic Engineering, Changsha University of Science & Technology, Changsha, 410114, China;

b. School for Marine Science and Technology, University of Massachusetts Dartmouth, New Bedford, MA 02744, USA;

c. Key Laboratory of Water-Sediment Sciences and Water Disaster Prevention of Hunan Province, Changsha, 410114, China;

d. Department of Mathematics, University of Massachusetts Dartmouth, North Dartmouth, MA 02747, USA.

## Highlights

- An SST predicting method based on the hybrid EMD algorithms and BP neural network method is proposed in this paper.
- SST prediction results based on the hybrid EEMD-BPNN and CEEMD-BPNN models are compared and discussed.
- Cases study of SST in the North Pacific shows that the proposed hybrid CEEMD-BPNN model can effectively predict the time-series SST.

**Abstract:** Sea surface temperature (SST) is the major factor that affects the ocean-atmosphere interaction, and in turn the accurate prediction of SST is the key to ocean dynamic prediction. In this paper, an SST predicting method based on empirical mode decomposition (EMD) algorithms and back-propagation neural network (BPNN) is proposed. Two different EMD algorithms have been applied extensively for analyzing time-series SST data and some nonlinear stochastic signals. Ensemble empirical mode decomposition (EEMD) algorithm and Complementary Ensemble Empirical Mode Decomposition (CEEMD) algorithm are two improved algorithms of EMD, which can effectively handle the mode-mixing problem and decompose the original data into more stationary signals with different frequencies. Each Intrinsic Mode Function (IMF) has been taken as input data to the back-propagation neural network model. The final predicted SST data is obtained by aggregating the predicted data of individual IMF<sub>i</sub>. A case study of the monthly mean SST anomaly (SSTA) in the northeastern region of the North Pacific, shows that the proposed hybrid CEEMD-BPNN model is much more accurate than the hybrid EEMD-BPNN model, and the prediction accuracy based on BP neural network is improved by the CEEMD method. Statistical analysis of the case study demonstrates

30 that applying the proposed hybrid CEEMD-BPNN model is effective for the SST prediction.

31

32 **Keywords.**

33 Sea Surface Temperature; Back-Propagation Neural Network; Empirical Mode Decomposition; Prediction;  
34 Machine Learning Algorithms.

35

36 **1 Introduction**

37 The Sea Surface Temperature (SST) is a main factor in the interaction between the ocean and the  
38 atmosphere (Wiedermann et al., 2017; He et al., 2017; Wu et al., 2019a), and it characterizes the combined  
39 results of ocean heat (Buckley et al., 2014; Griffies et al., 2015; Wu et al., 2019b) and dynamic processes  
40 (Takakura et al., 2018). It is a very important parameter for climate change and ocean dynamics processes,  
41 such as sea-air heat fluxes and water vapor exchange. Small changes in sea temperature can have a huge  
42 impact on the global climate. The well-known El Niño and La Niña phenomena are caused by abnormal  
43 changes in SST (Chen et al., 2016a; Zheng et al., 2016).

44 Therefore, scholars have begun to observe the SST in recent years, the observation of the SST is  
45 important (Kumar et al., 2017; Sukresno et al., 2018). Accurate observation and effective prediction of the  
46 SST are very important (Hudson et al., 2010). Predicting the SST in advance can enable people to take  
47 appropriate measures to reduce the impact on daily life and reduce unnecessary losses. However, due to the  
48 high randomness and irregularity of the monthly mean sea surface temperature anomaly (SSTA), the  
49 nonlinear and non-stationary characteristics are obvious. At present, there is no clear and feasible method  
50 with high accuracy to effectively predict the SST (Zhu et al., 2015; Chen et al., 2016b; Khan et al., 2017).

51 In mathematics and science, a nonlinear system is a system in which the change of the output is not  
52 proportional to the change of the input. Nonlinear dynamical systems, describing changes in variables over  
53 time, may appear chaotic, unpredictable, or counterintuitive, contrasting with much simpler linear systems.  
54 A stationary process is a stochastic process whose unconditional joint probability distribution does not change  
55 when shifted in time. Consequently, statistical parameters such as mean and variance also do not change over  
56 time. The variation of SST is a non-linear dynamic system with non-stationary time series data. Empirical  
57 Mode Decomposition (EMD) is a state-of-the-art signal processing method proposed by Huang et al. (1998).  
58 This method can decompose the signal data of different frequencies step by step according to the  
59 characteristics of the data and obtain several orthogonal components and a trending component (Wang et al.,

60 2015; Amezquita-Sanchez and Adeli,2015; Wang et al., 2016; Kim and Cho, 2016). The empirical mode  
61 decomposition (EMD) method is powerful and adaptive in analyzing nonlinear and non-stationary data sets.  
62 It provides an effective approach for decomposing a signal into a collection of so-called intrinsic mode  
63 functions (IMFs), which can be treated as empirical basis functions (Duan et al., 2016). However, there were  
64 some problems with the EMD method, such as mode mixing (Huang and Wu, 2008; Wu et al., 2008; Wu and  
65 Huang, 2009).

66 Once an intermittent signal appears in the actual signal, the EMD decomposition method will produce  
67 a Mode Mixing Problem. The Mode Mixing Problem causes the essential modal function (IMFs) to lose their  
68 physical meaning. The problem is manifested as either a single IMF consisting of widely disparate scales, or  
69 a signal of similar scale captured in different IMF's. To overcome mode mixing two noise assisted methods  
70 have emerged.

71 Wu and Huang (2009) proposed the Ensemble Empirical Mode Decomposition (EEMD) method by  
72 adding different white noise in each ensemble member to suppress mode mixing. Ensemble Empirical Mode  
73 Decomposition (EEMD) adds a fixed percentage of white noise to the signal before decomposing it. This  
74 step is repeated N times after which all results are averaged. EEMD improves the mode-mixing problem but  
75 it cannot completely reconstruct the input signal from the resulting components.

76 Yeh et al. (2010) added two opposite-signal white noises to the time-series data sequence, and proposed  
77 an improved algorithm, Complete Ensemble Empirical Mode Decomposition (CEEMD). Similarly the  
78 method decomposes the signal with N different noise realizations but here the results are averaged after each  
79 IMF is found. The decomposition effect is equivalent to EEMD, and the reconstruction error caused by adding  
80 white noise is reduced (Tang et al., 2015). CEEMD solves the mode mixing problem and it provides an exact  
81 reconstruction of the input signal. In contrast to the EEMD method, the CEEMD also ensures that the IMF  
82 set is quasi-complete and orthogonal. The CEEMD is a computationally expensive algorithm and may take  
83 significant time to run. At present, the EMD model and its improved algorithms have been widely used in  
84 many fields on ocean science, such as storm surge and sea level rise (Wu et al., 2011; Lee, 2013; Ezer and  
85 Atkinson, 2014), tidal amplitude (Cheng et al., 2017; Pan et al., 2018) and wave height (Duan et al., 2016;  
86 Sadeghifar et al., 2017; López et al., 2017). These studies and applications reflected that the EMD model and  
87 its improved algorithms can effectively reduce the complexity of the non-stationarity time-series data, which  
88 helps further analysis and processing.

89 For nonlinear prediction, the more commonly used methods are curve fitting (Motulsky and Ransnas,

90 1987), gray-box model (Pearson and Pottmann, 2000), homogenization function model (Monteiro et al.,  
91 2008), neural network (Deo et al., 2001; Wang et al, 2015; Kim et al., 2016) and so on. Among them, Back-  
92 Propagation Neural Network (BPNN) (Lee, 2004; Jain and Deo, 2006; Savitha and Al, 2017; Wang et al.,  
93 2018) has certain advantages in dealing with nonlinear problems, it is a basic machine learning algorithm  
94 and its principle is simple and operability is strong, so in ocean science and engineering it has been widely  
95 used.

96 In view of non-stationary and nonlinear monthly mean SST, the EEMD, CEEMD and BP neural network  
97 will be used here to study how to improve the accuracy of SST prediction. The hybrid EMD-BPNN models  
98 will be established for the prediction of SSTA in the northeastern region of the Pacific Ocean.

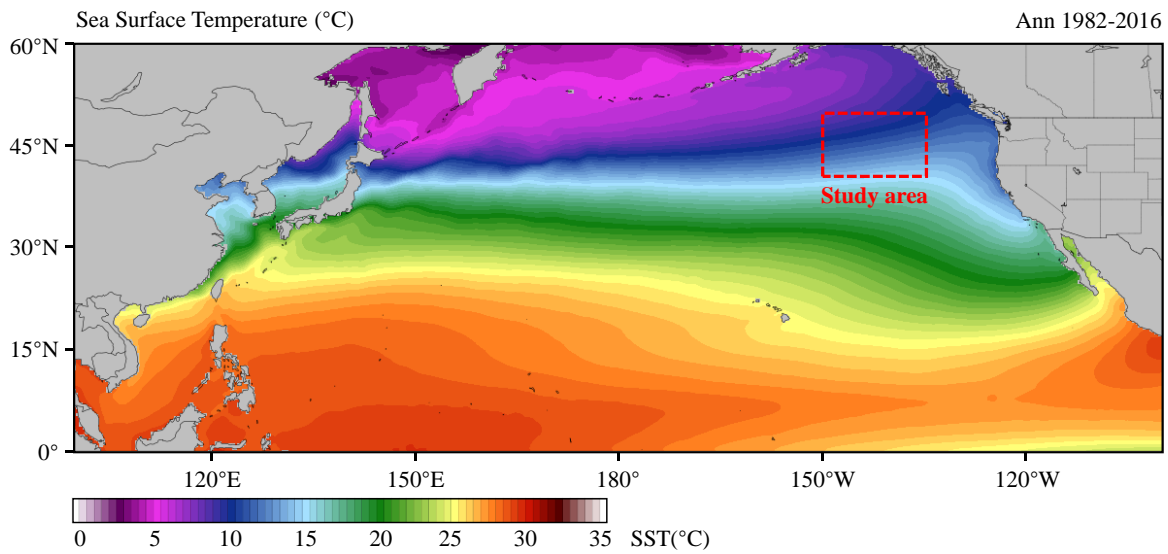
## 99 **2 Data collection**

100 Sea surface temperature (SST) is the temperature of the top millimeter of the ocean's surface. An  
101 anomaly is when something is different from normal, or average. A sea surface temperature anomaly (SSTA)  
102 is how different the ocean temperature at a particular location at a particular time is from the normal  
103 temperatures for that place. The monthly SSTA is the difference between the SST of this month and the  
104 average SST of all this month from 1982 to 2016. The annual SSTA is the difference between the average  
105 SST of this year and the average SST of 35 years from 1982 to 2016. For example, a global map of sea  
106 surface temperature anomaly for January 2016 would show where the temperatures in January 2016 were  
107 warmer, cooler, or the same as other Januarys in previous years. SSTAs can happen as part of normal ocean  
108 cycles or they can be a sign of long-term climate change, such as global warming. The SST time-series data  
109 in this study is from the NOAA Optimum Interpolation Sea Surface Temperature (OISST) official website  
110 (Reynolds et al., 2007; Banzon et al., 2016; <https://www.ncdc.noaa.gov/oisst/data-access>). The NOAA  
111 1/4°daily OISST is an analysis constructed by combining observations from different platforms (satellites,  
112 ships, buoys) on a regular global grid. There are two kinds of OISST, named after the relevant satellite SST  
113 sensors. These are the Advanced Very High Resolution Radiometer (AVHRR) and Advanced Microwave  
114 Scanning Radiometer on the Earth Observing System (AMSR-E); the AVHRR dataset is used in this study.  
115 The average annual sea surface temperature in North Pacific (0°N-60°N, 100°E-100°W) from January 1982  
116 to December 2016 is shown in Fig.1.

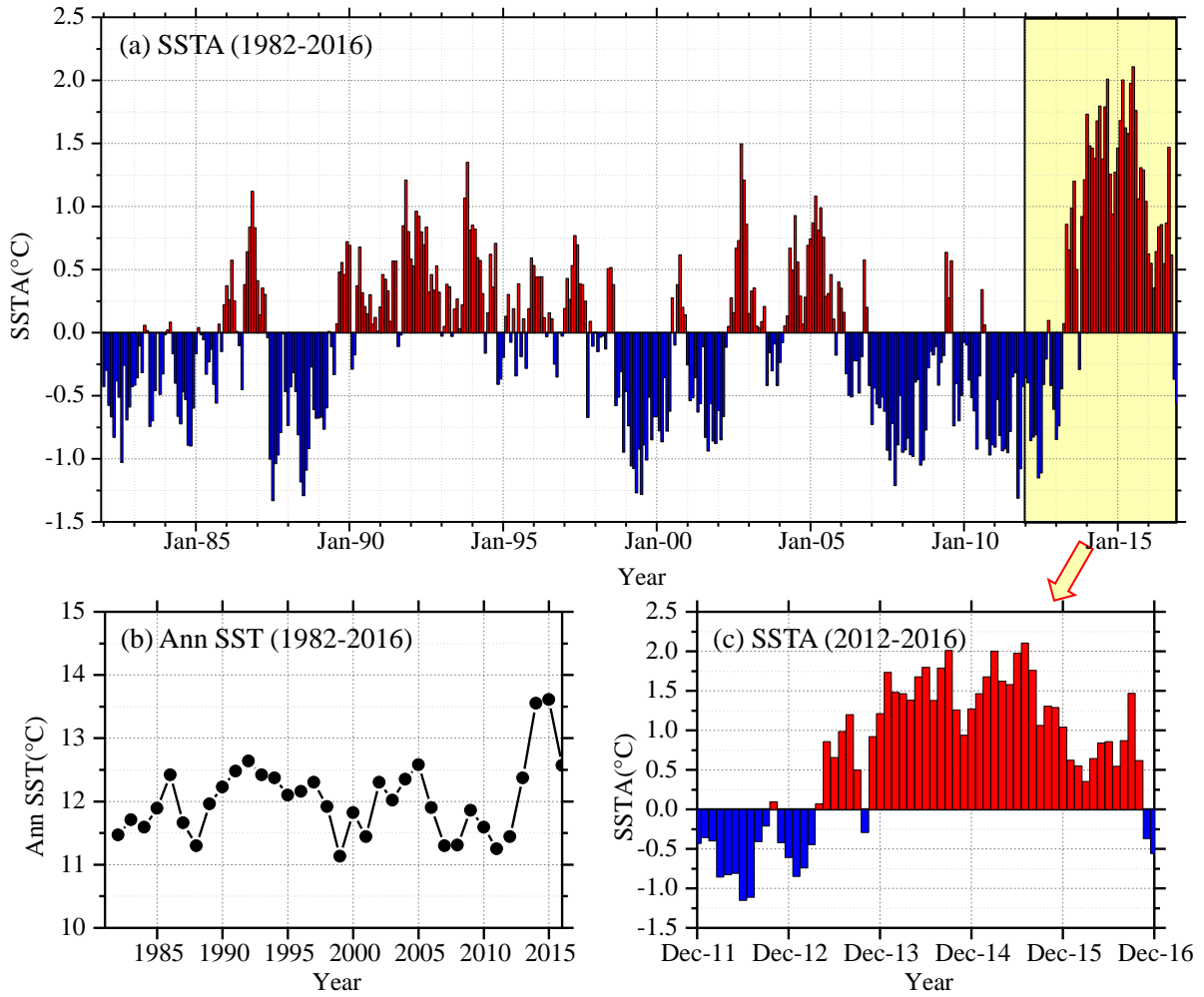
117 It has been shown that the sea surface temperature anomaly in the northeastern Pacific in the ten years  
118 2006-2016 was 2.0°C warmer than in the previous ten years 1996-2006. Previous studies (Bond et al., 2015)  
119 showed that in the spring and summer of 2014, the high SST area of the northeastern Pacific had expanded

120 to coastal ocean waters, which affected the weather in coastal areas and the lives of fishermen, and even  
121 affected the temperature in Washington, USA, causing interference to daily life.

122 In this study, we select the northeastern region of the North Pacific Ocean (in Fig.1, 40°N-50°N, 150°W-  
123 135°W) to measure SST. The time-series data of SST for the study area from January 1982 to December  
124 2016 with a data length of 420 months was obtained from OISST-V2 (Fig. 2). The monthly mean SSTA was  
125 used in the analysis and calculation. As shown in Fig. 2(a), the overall time-series data is very messy,  
126 nonlinear and random from the perspective of the image.



127 **Fig.1** Average sea surface temperature in North Pacific during Jan 1982 to Dec 2016 (35-years).  
128



129

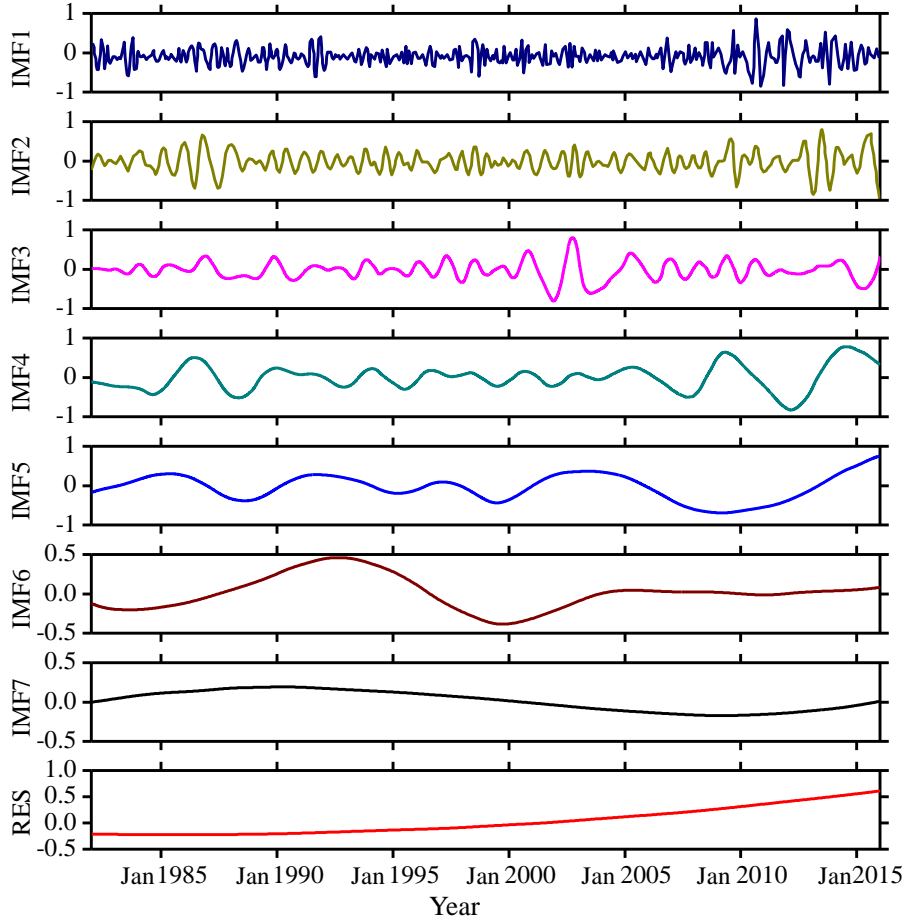
130 **Fig.2** The time-series of sea surface temperature in the study area. (a) SST anomaly (1982-2016, 35 years);  
 131 (b) Annual SST (1982-2016, 35 years); (c) SST anomaly (2012-2016, 5 years).

132 **3 Decomposition of SSTA**

133 The purpose of this study is to combine the EEMD algorithm and the CEEMD decomposition algorithm  
 134 respectively with the BP neural network algorithm to establish a prediction model, a hybrid EMD-BPNN  
 135 model. The EEMD and CEEMD algorithms are performed on the monthly mean SSTA data to obtain a series  
 136 of intrinsic mode functions (IMFi). Each IMFi is predicted by a BP neural network and then the IMFi are  
 137 recombined to obtain the predicted value of SSTA.

138 **3.1 Decomposition by the EEMD algorithm**

139 The SSTA in Fig. 2(a) has been decomposed based on the ensemble empirical mode decomposition  
 140 (EEMD algorithm), and seven IMF components and a residual component RES (Residue) are obtained as  
 141 shown in Fig. 3.



142

143 **Fig.3** IMF components and the trend item RES of monthly mean SSTA over the study area based on the  
 144 EEMD algorithm during 1982-2016.

145

146 It can be seen from Fig. 3 that the first three intrinsic mode function components IMF1, IMF2, and IMF3  
 147 still exhibit strong non-stationarity because they have strong irregular oscillations and periodic changes. The  
 148 IMF4 to IMF7 and the final trend term RES have some periodicity and relatively regular fluctuation, and the  
 149 non-stationary properties are less than the first three components. The trend term RES reflects that the overall  
 150 trend of SSTA has gradually increased since 1982. As the non-stationarity of  $IMF_i$  decreases with increasing  
 151  $i$ , the EEMD algorithm will reduce the influence of non-stationarity on prediction. The absolute error (ERR)  
 152 of the decomposition can be calculated by the following Formula (1).

153

$$a(t) = \left| S(t) - \left[ \sum_{i=1}^7 I_i(t) + R(t) \right] \right| \quad (1)$$

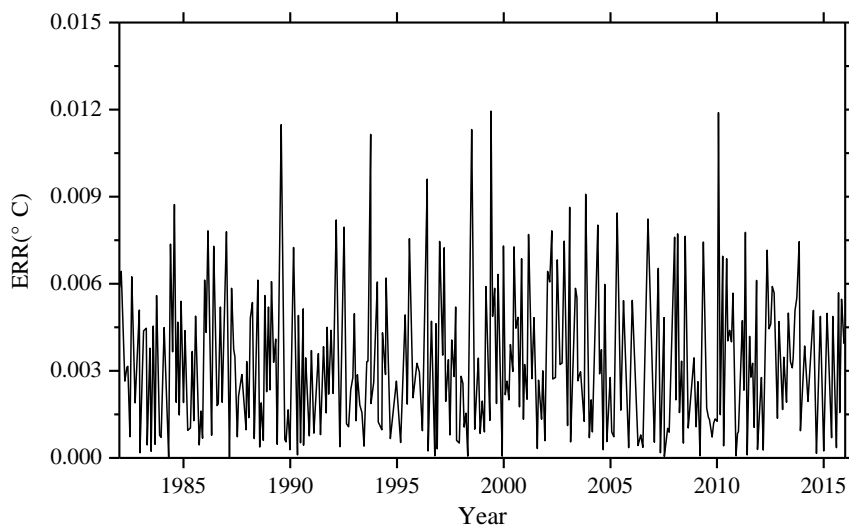
154

155

where,  $a(t)$  is the absolute error (ERR),  $S(t)$  the original SSTA observation data,  $I_i(t)$  the  $i$ -th component of the IMF ( $IMF_i$ ), and  $R(t)$  the trend term (RES).

156 The absolute error (ERR) based on the EEMD algorithm is shown in Fig. 4. It can be seen from the  
157 figure that the ERR of 420 months after decomposition is basically below 0.01 °C, and the ERR exceeds  
158 0.01 °C in five months: June 1989, September 1993, July 1998, May 1999 and March 2010.

159 In addition to June 1989, the other four monthly data with a large ERR occurred during the El Niño  
160 period. The maximum error is in March 2010, the actual value is -0.1204 °C, the result based on EEMD  
161 algorithm is -0.1325 °C, the ERR of decomposition is 0.0121 °C; the minimum error, in April 1987, is  
162  $1.73 \times 10^{-5}$  °C. The overall mean ERR based on the EEMD algorithm is 0.0035 °C.



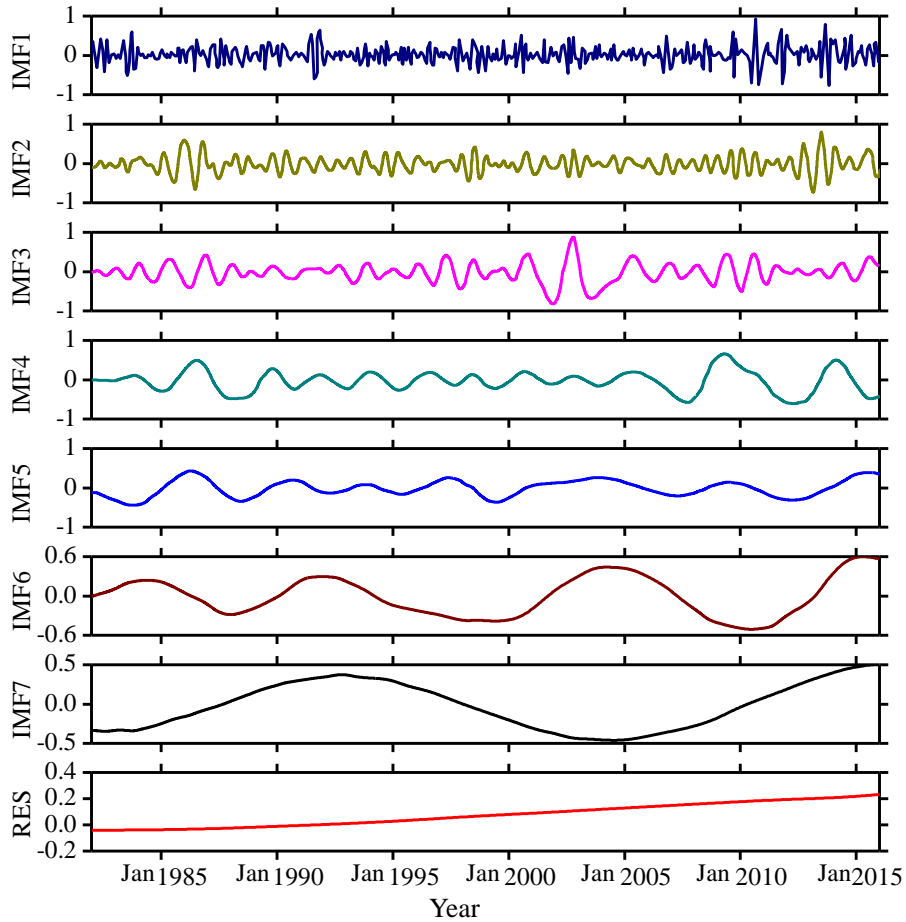
163  
164 **Fig. 4** The ERR of monthly mean SSTA over the study area based on the EEMD algorithm during 1982-2016.

165  
166

### 167 3.2 Decomposition by the CEEMD algorithm

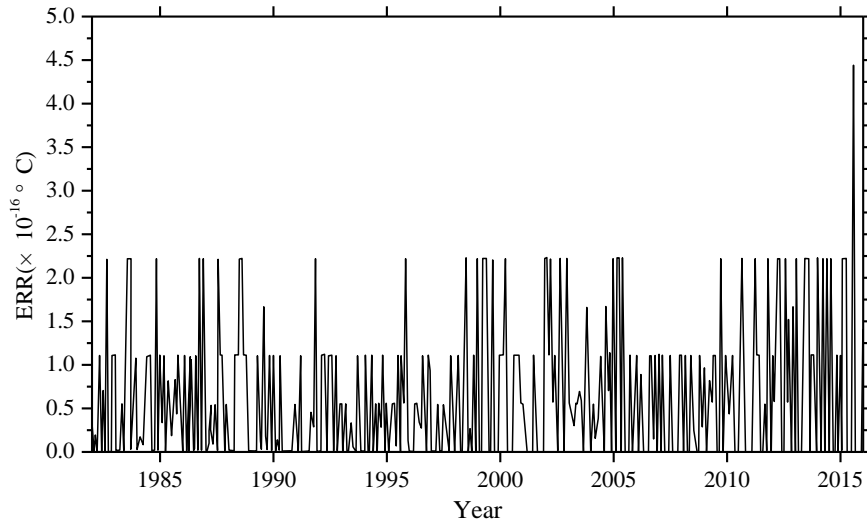
168 The SSTA has been decomposed based on the complementary ensemble empirical mode decomposition  
169 (CEEMD algorithm) and seven IMF components and a residual component RES (Residue) are obtained as  
170 shown in Fig. 5. It can be seen when comparing the decomposition results based on EEMD and CEEMD  
171 algorithms that although the mode components decomposed by CEEMD algorithm are different from the  
172 corresponding results decomposed by EEMD, the non-stationarities of the seven modes decomposed by the  
173 two decomposition algorithms are gradually decreasing, and the final trend term RES is an upward trend.  
174 Both decomposition algorithms confirm the characteristic of a gradual increase in the overall trend of the  
175 data series.





176  
 177 **Fig.5** IMF components and the trend item RES of monthly mean SSTA over the study area based on the  
 178 CEEMD algorithm during 1982-2016.

179  
 180 The absolute error (ERR) obtained based on the CEEMD algorithm is shown in Fig. 6. It can be seen  
 181 from the figure that the ERR of 420 months data after decomposition is less than  $5 \times 10^{-16} \text{ }^\circ\text{C}$ , and the accuracy  
 182 is much better. The maximum error is  $4.48 \times 10^{-16} \text{ }^\circ\text{C}$  in March 2016; the minimum error is zero. The overall  
 183 mean ERR based on CEEMD algorithm is  $6.10 \times 10^{-17} \text{ }^\circ\text{C}$ . By comparing the results and errors of the above  
 184 two decomposition algorithms, it can be seen that the error based on the improved algorithm (CEEMD) is  
 185 much smaller than the error based on the EEMD algorithm. Because more white noise with the opposite  
 186 sign had been added in CEEMD algorithm, the reconstruction error caused by the white noise has been  
 187 reduced compared with that of the EEMD algorithm.



188

189 **Fig. 6** The ERR of monthly mean SSTA over the study area based on the CEEMD algorithm during 1982-  
 190 2016.

191

192 **4 SSTA prediction model**

193 **4.1 The BP neural network**

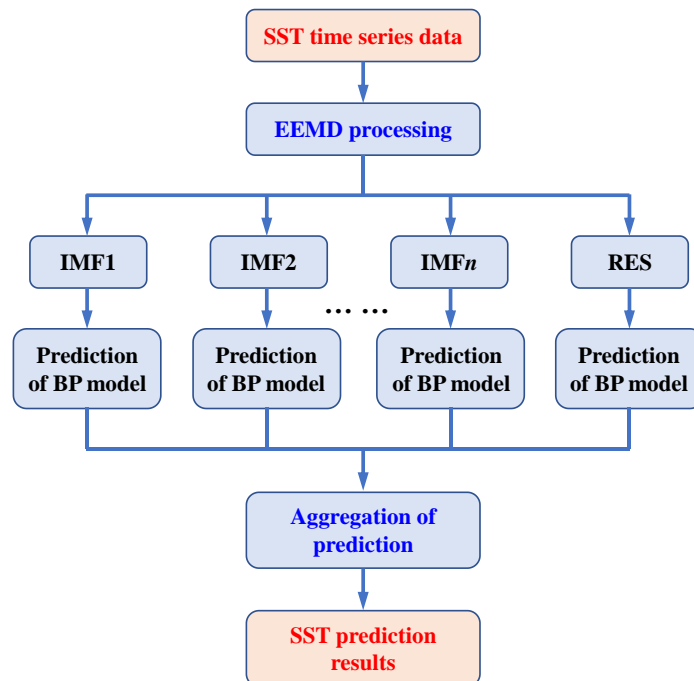
194 Artificial Neural Network (ANN) is an information processing approach based on the biological neural  
 195 network (López et al., 2015; Kim et al., 2016). In theory, ANN can simulate any complex nonlinear  
 196 relationship through nonlinear units (neurons) and has been widely used in the prediction area, such as wave  
 197 height and storm surge. The most basic structure of ANN consists of input layers, hidden layers and output  
 198 layers. One of the most widely used ANN models is the back propagation neural network (BPNN, Wang et  
 199 al., 2018) algorithm based on the BP algorithm.

200 The BPNN algorithm is a multi-layer feedforward network trained according to the error back  
 201 propagation algorithm and is one of the most widely used deep learning algorithms. The BP network can be  
 202 used to learn and store a large number of mappings of input and output models without the need to publicly  
 203 describe the mathematical equations of these mapping relationships. The learning rule is to use the steepest  
 204 descent method. When applied to SST predicting, the input data are monthly mean SST in previous months  
 205 and the output data are predicted SST time-series data. The desired data for comparison is the observed actual  
 206 SST.

207 **4.2 SSTA prediction model based on hybrid improved EMD-BPNN algorithm**

208 The proposed monthly mean sea surface temperature anomaly (SSTA) predicting model includes three

209 steps as follows. First, original SST datasets are decomposed into certain more stationary signals with  
 210 different frequencies by EEMD. Second, the BP neural network is used to predict each IMF and the residue  
 211 RES. A rolling forecasting process is studied. The prediction is made using the previous data for one step  
 212 ahead. Finally, the prediction results of each IMF and the residue RES are aggregated to obtain the final SST  
 213 prediction results. The flowchart of the SST prediction model based on hybrid improved empirical mode  
 214 decomposition algorithm (improved EMD algorithm) and back-propagation neural network (BPNN) is shown  
 215 in Fig. 7. The SST prediction model has been abbreviated as a hybrid improved EMD-BPNN model in the  
 216 following article.



217  
 218 **Fig.7** The flowchart of SST prediction model based on hybrid improved empirical mode decomposition  
 219 algorithm (improved EMD algorithm) and back-propagation neural network (BPNN).

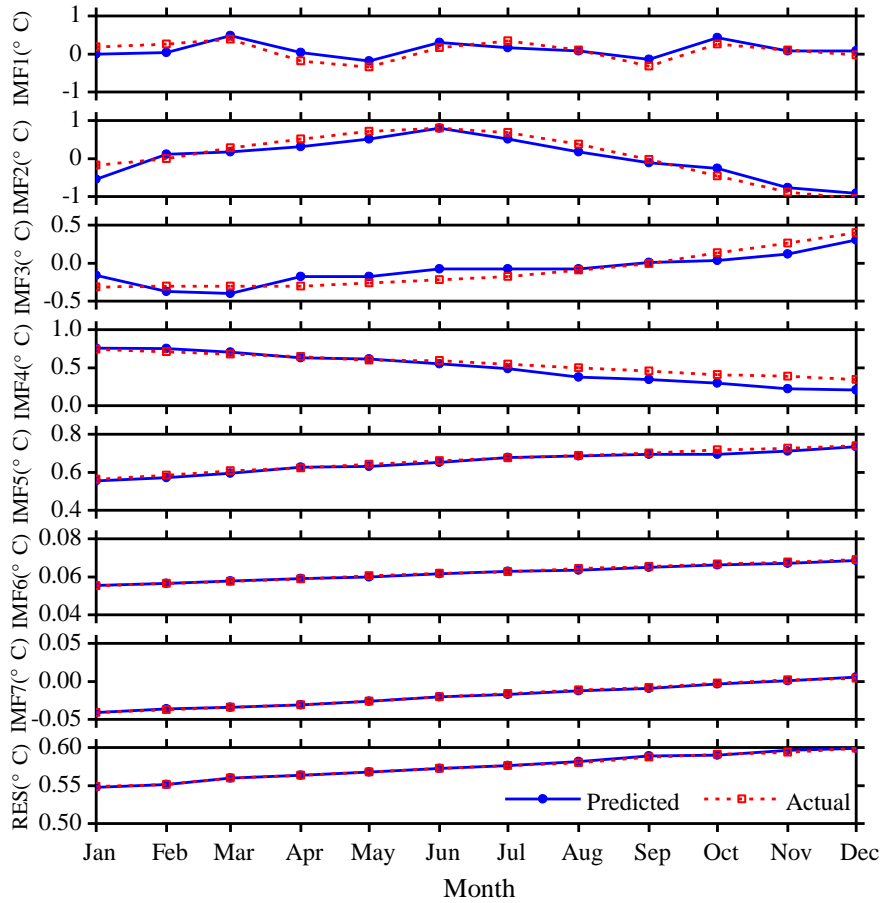
220  
 221

222 **5 Case study: SSTA prediction based on the hybrid improved EMD-BPNN models**

223 In order to study the effects of the two improved EMD algorithms (EEMD and CEEMD) on the  
 224 prediction results, and to analyze the prediction ability of BP neural network, the following experiments were  
 225 carried out. Predict SSTA results in 2017 and analyze the prediction abilities of different mode decomposition  
 226 data based on EEMD and CEEMD algorithms. The experiment content is as follows: the BP neural network  
 227 is trained with the decomposition data of each mode based on the datasets from 1982 to 2016, and then the

228 SSTA in 2017 is predicted by the trained neural network. The actual results of 12 months in 2017 based on  
 229 the observation are used to compare and analyze with the prediction results. Time-series SST data from 1982  
 230 to 2017 in the study zone are used in this case study, which are decomposed by EEMD and CEEMD into 8  
 231 different IMFs and the residue RES as shown in Fig. 8 and Fig.9 respectively.

232 A three-layer BP neural network structure has been chosen and independently analyze and predict each  
 233 month. For the IMF4 and subsequent modes, the non-stationarity have been degraded relative to the first  
 234 three modes, a BP neural network with 12 nodes at input layer and output layer has been used to train and  
 235 predict SSTA. The prediction results of each mode decomposition component based on the EEMD algorithm  
 236 are shown in Fig. 8. The absolute errors of the predicted value and the actual value are shown in Table 1.



237  
 238 **Fig. 8** SSTA prediction results based on the hybrid EEMD-BPNN model of each individual component in  
 239 2017.

240 Root mean square error (RMSE) is used as metrics to access the performance of the two different models.

$$241 \quad \text{RMSE} = \sqrt{\frac{1}{N} \sum_{n=1}^N (x_n - y_n)^2} \quad (2)$$

242 where,  $x_n$  and  $y_n$  are the observed and the predicted values respectively,  $N$  is the number of data used for

243 the performance evaluation and  $N$  is 12 in this study. Results are shown in Table 1.

244

245 **Table 1.** The absolute errors ERRs of the SSTA prediction results of each individual component based on the  
246 hybrid EEMD-BPNN model (unit: °C).

	Max ERR	Min ERR	Mean ERR	RMSE
IMF1	0.2197	0.0014	0.1424	0.1486
IMF2	0.2166	0.0323	0.1297	0.1673
IMF3	0.1872	0.0051	0.1070	0.1245
IMF4	0.1602	$1.6869 \times 10^{-4}$	0.0663	0.0857
IMF5	0.0158	0.0010	0.0089	0.0104
IMF6	$3.8766 \times 10^{-4}$	$1.9752 \times 10^{-4}$	$2.7221 \times 10^{-4}$	0.0003
IMF7	$5.2662 \times 10^{-4}$	$1.6387 \times 10^{-4}$	$1.7907 \times 10^{-4}$	0.0002
RES	$5.4859 \times 10^{-4}$	$2.2308 \times 10^{-4}$	$2.7766 \times 10^{-4}$	0.0003

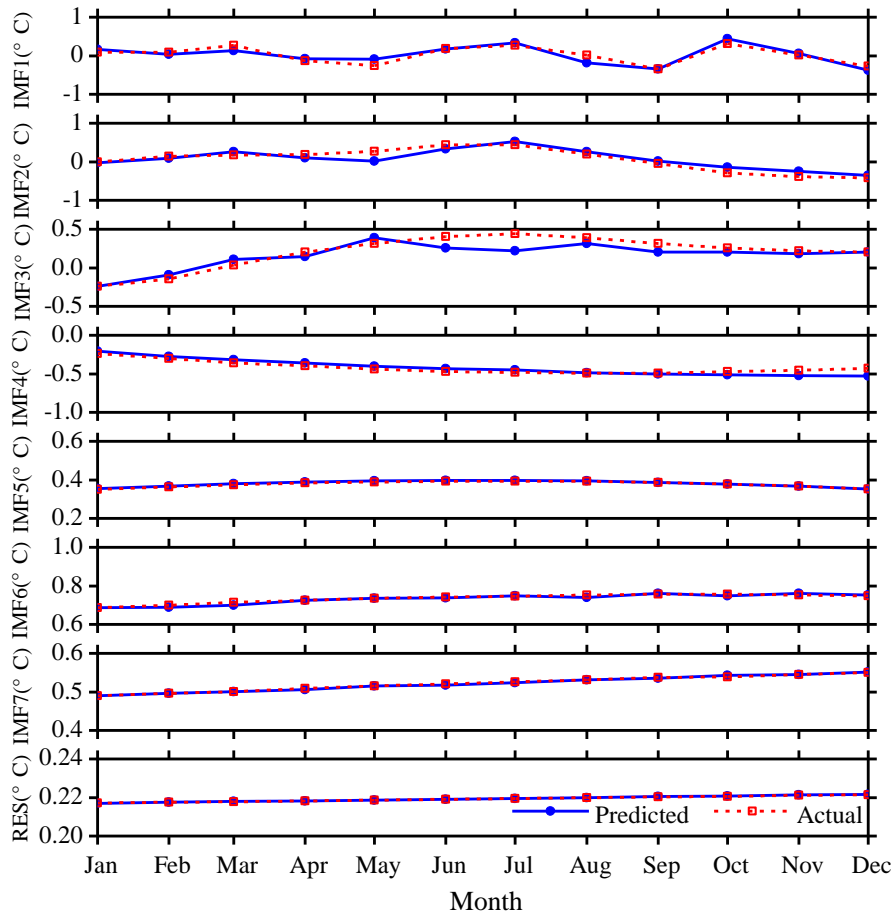
247

248 It can be seen from Fig. 8 and Table 1 that the maximum absolute error (Max ERR) of the first  
249 decomposition component IMF1 based on the hybrid EEMD-BPNN model is 0.2197 °C in January. The  
250 minimum absolute error (Min ERR) is 0.0014 °C, which is in August. The prediction ability of the second  
251 mode decomposition component IMF2 is roughly equivalent to the IMF1, and the mean absolute error (Mean  
252 ERR) of the first three intrinsic mode function components IMF1, IMF2, and IMF3 are between 0.10 °C and  
253 0.15 °C. The mean absolute errors of the IMF4 and IMF5 are 0.0663 °C and 0.0089 °C, respectively, and the  
254 prediction accuracy based on the hybrid EEMD-BPNN model is roughly equivalent to the decomposition  
255 accuracy of the EEMD algorithm. The prediction errors of the last two intrinsic mode function components  
256 and the residue RES are on the order of  $10^{-4}$ . It can be seen that as the non-stationarity of the series data  
257 decreases, the error of the prediction results becomes smaller and smaller.

258 According to the same method, the eight mode components decomposed by CEEMD algorithm have  
259 been analyzed and predicted. The prediction results and error analysis have been shown in Fig. 9 and Table  
260 2. It can be seen from Fig. 9 and Table 2 that the maximum error of the first decomposition component IMF1  
261 based on the hybrid CEEMD-BPNN model is 0.1779 °C in May. The minimum error is 0.0068 °C, which is  
262 in June.

263 The prediction ability of the second mode decomposition component IMF2 is roughly equivalent to the

264 IMF1. Except for the four months of May, September, October, and November, the accuracies of prediction  
 265 results of other months are satisfactory. The prediction results of the first three intrinsic mode function  
 266 components IMF1, IMF2, and IMF3 are basically the same as the actual data. In the prediction results of the  
 267 fourth mode component IMF4, except for a slight error in December, the prediction ability is better. The  
 268 predicted results of the last three intrinsic mode function components IMF5, IMF6, IMF7 and the residue  
 269 RES are basically consistent with the observation results.

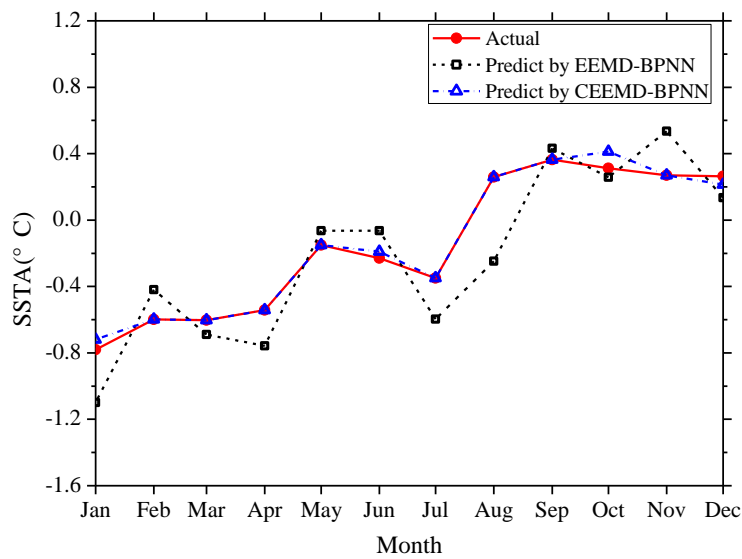


270  
 271 **Fig. 9** SSTA prediction results based on the hybrid CEEMD-BPNN model of each individual component in  
 272 2017.  
 273

274 **Table 2.** The absolute errors ERRs of the SSTA prediction results of each individual component based on the  
 275 hybrid CEEMD-BPNN model (unit: °C).

	Max ERR	Min ERR	Mean ERR	RMSE
IMF1	0.1779	0.0068	0.0827	0.0987
IMF2	0.1643	0.0413	0.0811	0.1124
IMF3	0.1521	0.0160	0.0713	0.1006
IMF4	0.0851	0.0211	0.0324	0.0427
IMF5	0.0052	$8.7694 \times 10^{-5}$	0.0021	0.0029
IMF6	0.0103	$5.7748 \times 10^{-5}$	0.0043	0.0056
IMF7	0.0017	$3.6026 \times 10^{-5}$	$9.1374 \times 10^{-4}$	0.0010
RES	$3.0342 \times 10^{-5}$	$2.0163 \times 10^{-6}$	$1.1572 \times 10^{-5}$	$1.5017 \times 10^{-5}$

276  
 277 The prediction results of the monthly mean SSTA in 2017 are obtained by reconstructing the mode  
 278 decomposition components (Fig. 10) and the absolute error (ERR) of prediction results have been shown in  
 279 Table 3. It can be seen from the figure and table that the prediction results based on the EEMD-BPNN model  
 280 have larger ERRs in January and August, exceeding 0.3 °C, and the accuracies of prediction results in other  
 281 months are satisfactory (the ERR is less than 0.3). The prediction accuracy based on the CEEMD-BPNN  
 282 model is more satisfactory, ERR exceeds 0.1 °C only in October, and the prediction ability based on the  
 283 CEEMD-BPNN model is generally better than that of the EEMD-BPNN model.



284  
 285 **Fig. 10** Monthly SSTA prediction results based on the hybrid improved EMD-BPNN models in 2017.

286 **Table 3.** The absolute errors ERRs of the SSTA prediction results based on the two different hybrid improved  
 287 EMD-BPNN models (unit: °C).

	EEMD-BPNN model	CEEMD-BPNN model		EEMD-BPNN model	CEEMD-BPNN model
Jan	0.3188	0.0623	Sep	0.0687	0.0132
Feb	0.1780	0.0103	Oct	0.0545	0.1607
Mar	0.0867	0.0063	Nov	0.2651	0.0101
Apr	0.2153	0.0137	Dec	0.1290	0.0183
May	0.0854	0.0102	<b>Min ERR</b>	<b>0.0545</b>	<b>0.0063</b>
Jun	0.1662	0.0224	<b>Max ERR</b>	<b>0.5068</b>	<b>0.1607</b>
Jul	0.2474	0.0077	<b>Mean ERR</b>	<b>0.1935</b>	<b>0.0289</b>
Aug	0.5068	0.0112	<b>RMSE</b>	<b>0.2299</b>	<b>0.0512</b>

288  
 289 The correlation coefficient between the prediction values based on the CEEMD-BPNN model and  
 290 observations is 0.97 indicating a significance level of 0.001. The result indicates that SSTA in 2017 was  
 291 predicted accurately by the CEEMD-BPNN model. As can be seen from the above discussions, the ERR of  
 292 decomposition components based on the EEMD and CEEMD algorithms will affect the accuracy of the final  
 293 prediction results. Table 3 shows that prediction results of the hybrid CEEMD and BPNN model are much  
 294 better than with the EEMD-BPNN. This is because after CEEMD, the original unsteady data are changed  
 295 into certain components that have fixed frequency and periodicity. The CEEMD algorithm with less  
 296 decomposition error has less error in the final prediction results, which proves that the CEEMD method has  
 297 more advantages in data decomposition than the EEMD method. At the same time, we can find that the final  
 298 prediction error of the two prediction models mainly comes from the first three mode decomposition  
 299 components, and the error of the last five components has little effect on the accuracy of the final prediction  
 300 results.

301  
 302 **6 Conclusions**

303 This paper presents an SST predicting method based on the hybrid EMD algorithms and BP neural  
 304 network method to process the SST data with nonlinearity and non-stationarity. Through EEMD and CEEMD  
 305 algorithms, SSTA time-series data are decomposed into different IMFs and a residue RES. BP neural network  
 306 is applied to predict individual IMFs and the residue RES. Final results can be obtained by adding the



307 predicting results of individual IMFs and RES.

308 In order to illustrate the effectiveness of the proposed approach, a case study was carried out. SSTA  
309 prediction results based on the hybrid EEMD-BPNN model and the hybrid CEEMD-BPNN model are  
310 discussed. In comparison, the proposed hybrid CEEMD-BPNN model is much better and its prediction results  
311 are more accurate.

312 From the absolute error of the prediction results of each component IMF and the absolute error of the  
313 predicted SSTA, the prediction error of SSTA mainly comes from the prediction of the first three mode  
314 decomposition components (IMF1, IMF2 and IMF3). SST prediction has been only preliminary, based on  
315 the two improved EMD algorithms and BP neural network in this paper. The results show that the hybrid  
316 CEEMD-BPNN model is more accurate in predicting SST. This work can provide a reference for predicting  
317 SST and El Niño in the future. In a follow-up study, how to improve the forecast duration is the focus.

318 It should be noted that some factors affecting the SST prediction results include: the length and interval  
319 of the time series of the database, as well as different data sources because their values are also different. The  
320 SST time-series data in this study is based on NOAA Optimum Interpolation Sea Surface Temperature  
321 (OISST) datasets from January 1982 to December 2016.

322

### 323 **Acknowledgement**

324 This work was supported by National Natural Science Foundation of China (Grant Nos. 51809023,  
325 51879015, 51839002, 51809021 and 51509023). The authors are grateful to Prof. John M. Huthnance for his  
326 careful checking, comments and valuable input.

327

### 328 **References:**

329 Amezquita-Sanchez, J. P. and Adeli, H.: A new music-empirical wavelet transform methodology for time–  
330 frequency analysis of noisy nonlinear and non-stationary signals, *Digit. Signal Process.*, 45, 55-68,  
331 <https://doi.org/10.1016/j.dsp.2015.06.013>, 2015.

332 Banzon, V., Smith, T. M., Chin, T. M., Liu, C., and Hankins, W.: A long-term record of blended satellite and  
333 in situ sea-surface temperature for climate monitoring, modeling and environmental studies, *Earth Syst.*  
334 *Sci. Data*, 8, 165-176, <https://doi.org/10.5194/essd-8-165-2016>, 2016.

335 Bond, N. A., Cronin, M. F., Freeland, H., and Mantua N.: Causes and impacts of the 2014 warm anomaly in  
336 the NE Pacific. *Geophys. Res. Lett.*, 42, 3414-3420, <https://doi.org/10.1002/2015GL063306>, 2015.

337 Buckley, M. W., Ponte, R. M., Forget, G., and Heimbach, P.: Low-frequency SST and upper-ocean heat  
338 content variability in the North Atlantic, *J. Climate*, 27, 4996-5018, [https://doi.org/10.1175/JCLI-D-13-](https://doi.org/10.1175/JCLI-D-13-00316.1)  
339 00316.1, 2014.

340 Chen, C., Cane, M. A., Henderson, N., Lee, D. E., Chapman, D., Kondrashov D., and Chekroun, M. D.:  
341 Diversity, nonlinearity, seasonality, and memory effect in ENSO simulation and prediction using  
342 empirical model reduction, *J. Climate*, 29: 1809-1830, <https://doi.org/10.1175/JCLI-D-15-0372.1>,  
343 2016b.

344 Chen, Z., Wen, Z., Wu, R., Lin X., and Wang J.: Relative importance of tropical SST anomalies in maintaining  
345 the Western North Pacific anomalous anticyclone during El Niño to La Niña transition years, *Clim.*  
346 *Dynam.*, 46, 1027-1041, <https://doi.org/10.1007/s00382-015-2630-1>, 2016a.

347 Cheng, Y., Ezer, T., Atkinson, L. P., and Xu, Q.: Analysis of tidal amplitude changes using the EMD method,  
348 *Cont. Shelf Res.*, 148: 44-52, <https://doi.org/10.1016/j.csr.2017.09.009>, 2017.

349 Deo, M. C., Jha, A., Chaphekar, A. S., and Ravikant, K.: Neural networks for wave forecasting, *Ocean Eng.*,  
350 28: 889-898, [https://doi.org/10.1016/S0029-8018\(00\)00027-5](https://doi.org/10.1016/S0029-8018(00)00027-5), 2001.

351 Duan, W. Y., Han, Y., Huang, L. M., Zhao, B. B., and Wang, M. H.: A hybrid EMD-SVR model for the short-  
352 term prediction of significant wave height, *Ocean Eng.*, 124, 54-73,  
353 <https://doi.org/10.1016/j.oceaneng.2016.05.049>, 2016.

354 Duan, W., Huang, L., Han Y., and Huang D.: A hybrid EMD-AR model for nonlinear and non-stationary  
355 wave forecasting, *J Zhejiang Univ-Sc A*, 17(2): 115-129, <https://doi.org/10.1631/jzus.A1500164>, 2016.

356 Ezer, T. and Atkinson, L. P.: Accelerated flooding along the US East Coast: on the impact of sea - level rise,  
357 tides, storms, the Gulf Stream, and the North Atlantic oscillations, *Earths Future*, 2, 362-382,  
358 <https://doi.org/10.1002/2014EF000252>, 2014.

359 Griffies, S. M., Winton, M., Anderson, W. G., Benson, R., Delworth, T. L., Dufour, C. O., Dunne, J. P.,  
360 Goddard, P., Morrison, A. K., Rosati, A., Wittenberg, A. T., Yin, J., and Zhang, R.: Impacts on ocean  
361 heat from transient mesoscale eddies in a hierarchy of climate models. *J. Climate*, 28, 952-977,  
362 <https://doi.org/10.1175/JCLI-D-14-00353.1>, 2015.

363 He, J., Deser, C., and Soden, B. J.: Atmospheric and oceanic origins of tropical precipitation variability. *J.*  
364 *Climate*, 30, 3197-3217, <https://doi.org/10.1175/JCLI-D-16-0714.1>, 2017.

365 Huang, N. E., Shen, Z., Long, S. R., Wu, M. C., Shih, H. H., Zheng, Q., Yen, N., Tung, C. C., and Liu, H. H.:  
366 The empirical mode decomposition and the Hilbert spectrum for nonlinear and non-stationary time

367 series analysis, *P. Roy. Soc. A-Math. Phys.*, 454, 903-995. <https://doi.org/10.1098/rspa.1998.0193>, 1998.

368 Huang, N. E. and Wu, Z.: A review on Hilbert - Huang transform: Method and its applications to geophysical  
369 studies, *Rev. Geophys.*, 46, RG2006, <https://doi.org/10.1029/2007RG000228>, 2008.

370 Hudson, D., Alves, O., Hendon, H. H., Wang, G.: The impact of atmospheric initialisation on seasonal  
371 prediction of tropical Pacific SST, *Clim. Dynam.*, 36, 1155-1171, [https://doi.org/10.1007/s00382-010-](https://doi.org/10.1007/s00382-010-0763-9)  
372 0763-9, 2011.

373 Jain, P. and Deo, M. C.: Neural networks in ocean engineering, *Ships Offshore Struc.*, 1, 25-35,  
374 <https://doi.org/10.1533/saos.2004.0005>, 2006.

375 Khan, M. Z. K., Sharma, A., and Mehrotra, R.: Global seasonal precipitation forecasts using improved sea  
376 surface temperature predictions, *J Geophys. Res. -Atmos.*, 122, 4773-4785,  
377 <https://doi.org/10.1002/2016JD025953>, 2017,

378 Kim, Y., Kim, H., and Ahn, I. G.: A study on the fatigue damage model for Gaussian wideband process of  
379 two peaks by an artificial neural network, *Ocean Eng.*, 111, 310-322,  
380 <https://doi.org/10.1016/j.oceaneng.2015.11.008>, 2016.

381 Kumar, M., Parmar, C., Chaudhary, V., Kumar, A., and SST-1 team.: Observation of plasma shift in SST-1  
382 using optical imaging diagnostics, *J Phys. Conf. Ser.*, 823, 012056, [https://doi.org/10.1088/1742-](https://doi.org/10.1088/1742-6596/823/1/012056)  
383 6596/823/1/012056, 2017.

384 Lee, H. S.: Estimation of extreme sea levels along the Bangladesh coast due to storm surge and sea level rise  
385 using EEMD and EVA, *J Geophys. Res.-Oceans*, 118, 4273-4285, <https://doi.org/10.1002/jgrc.20310>,  
386 2013,

387 Lee, T. L.: Back-propagation neural network for long-term tidal predictions, *Ocean Eng.*, 31, 225-238,  
388 [https://doi.org/10.1016/S0029-8018\(03\)00115-X](https://doi.org/10.1016/S0029-8018(03)00115-X), 2004.

389 López, I., Aragonés, L., Villacampa, Y., and Serra, J. C.: Neural network for determining the characteristic  
390 points of the bars, *Ocean Eng.*, 136: 141-151, <https://doi.org/10.1016/j.oceaneng.2017.03.033>, 2017.

391 Monteiro, E., Yvonnet, J., He, Q. C.: Computational homogenization for nonlinear conduction in  
392 heterogeneous materials using model reduction. *Comp. Mater. Sci.*, 42, 704-712,  
393 <https://doi.org/10.1016/j.commatsci.2007.11.001>, 2008.

394 Motulsky, H. J. and Ransnas, L. A.: Fitting curves to data using nonlinear regression: a practical and  
395 nonmathematical review, *Faseb J.*, 1, 365-374. <https://doi.org/10.1096/fasebj.1.5.3315805>, 1987.

396 Pan, H., Guo, Z., Wang, Y., and Lv, X.: Application of the EMD method to river tides, *J. Atmos. Ocean. Tech.*,

397 35, 809-819, <https://doi.org/10.1175/JTECH-D-17-0185.1>, 2018.

398 Pearson, R. K. and Pottmann, M.: Gray-box identification of block-oriented nonlinear models, *J. Process*  
399 *Contr.*, 10, 301-315, [https://doi.org/10.1016/S0959-1524\(99\)00055-4](https://doi.org/10.1016/S0959-1524(99)00055-4), 2000.

400 Reynolds, R. W., Smith, T. M., Liu, C., Chelton, D. B., Casey, K. S., and Schlax., M. G.: Daily high-  
401 resolution-blended analyses for sea surface temperature, *J. Climate*, 20, 5473-5496,  
402 <https://doi.org/10.1175/2007JCLI1824.1>, 2007.

403 Sadeghifar, T., Motlagh, M. N., Azad, M. T., and Mahdizadeh, M. M.: Coastal wave height prediction using  
404 Recurrent Neural Networks (RNNs) in the south Caspian Sea, *Mar. Geod.*, 40, 454-465,  
405 <https://doi.org/10.1080/01490419.2017.1359220>, 2017.

406 Savitha, R. and Mamun, A. A.: Regional ocean wave height prediction using sequential learning neural  
407 networks, *Ocean Eng.*, 129: 605-612, <https://doi.org/10.1016/j.oceaneng.2016.10.033>, 2017.

408 Sukresno, B., Hanintyo, R., Kusuma, D. W., Jatisworo, D., and Murdimanto., A.: Three-way error analysis  
409 of sea surface temperature (SST) between HIMAWARI-8, buoy, and mur SST in SAVU Sea, *Int. J.*  
410 *Remote Sens. Earth Sci.*, 15, 25-36, <https://doi.org/10.30536/j.ijreses.2018.v15.a2855>, 2018,

411 Takakura, T., Kawamura, R., Kawano, T., Ichiyangi, K., Tanoue, M., and Yoshimura, K.: An estimation of  
412 water origins in the vicinity of a tropical cyclone's center and associated dynamic processes, *Clim.*  
413 *Dynam.*, 50, 555-569, <https://doi.org/10.1007/s00382-017-3626-9>, 2018.

414 Tang, L., Dai, W., Yu, L., and Wang, S.: A novel CEEMD-based EELM ensemble learning paradigm for crude  
415 oil price forecasting, *Int. J. Inf. Tech. Decis.*, 14, 141-169, <https://doi.org/10.1142/S0219622015400015>,  
416 2015.

417 Wang, S., Zhang, N., Wu, L., and Wang, Y.: Wind speed forecasting based on the hybrid ensemble empirical  
418 mode decomposition and GA-BP neural network method, *Renew. Energ.*, 94, 629-636,  
419 <https://doi.org/10.1016/j.renene.2016.03.103>, 2016.

420 Wang, W., Chau, K., Xu, D., and Chen, X.: Improving forecasting accuracy of annual runoff time series using  
421 ARIMA based on EEMD decomposition, *Water Resour. Manag.*, 29, 2655-2675,  
422 <https://doi.org/10.1007/s11269-015-0962-6>, 2015.

423 Wang, W., Tang, R., Li, C., Liu, P., and Luo, L.: A BP neural network model optimized by Mind Evolutionary  
424 Algorithm for predicting the ocean wave heights, *Ocean Eng.*, 162, 98-107,  
425 <https://doi.org/10.1016/j.oceaneng.2018.04.039>, 2018.

426 Wang, Y., Wilson, P. A., Zhang, M., and Liu, X.: Adaptive neural network-based backstepping fault tolerant

427 control for underwater vehicles with thruster fault, *Ocean Eng.*, 110, 15-24,  
428 <https://doi.org/10.1016/j.oceaneng.2015.09.035>, 2015.

429 Wiedermann, M., Donges, J. F., Handorf, D., Kurths, J., and Donner, R. V.: Hierarchical structures in  
430 Northern Hemispheric extratropical winter ocean–atmosphere interactions, *Int. J. Climatol.*, 37, 3821-  
431 3836, <https://doi.org/10.1002/joc.4956>, 2017.

432 Wu, L. C., Kao, C. C., Hsu, T. W., Jao K. C. and Wang, Y. F.: Ensemble empirical mode decomposition on  
433 storm surge separation from sea level data, *Coast. Eng. J.*, 53, 223-243,  
434 <https://doi.org/10.1142/S0578563411002343>, 2011.

435 Wu Z., Schneider E. K. and Kirtman B. P.: The modulated annual cycle: an alternative reference frame for  
436 climate anomalies, *Clim. Dyna.*, 31(7-8): 823-841, <https://doi.org/10.1007/s00382-008-0437-z>, 2008.

437 Wu, Z. and Huang, N. E.: Ensemble empirical mode decomposition: a noise-assisted data analysis method,  
438 *Adv. Adap. Data Anal.*, 1, 1-41, <https://doi.org/10.1142/S1793536909000047>, 2009.

439 Wu Z., Jiang C., Chen J., Long Y., Deng B. and Liu X.: Three-Dimensional Temperature Field Change in the  
440 South China Sea during Typhoon Kai-Tak (1213) Based on a Fully Coupled Atmosphere–Wave–Ocean  
441 Model, *Water*, 11(1): 140, <https://doi.org/10.3390/w11010140>, 2019a.

442 Wu Z., Jiang C., Deng B., Chen J., Long Y., Qu K. and Liu X.: Numerical investigation of Typhoon Kai-tak  
443 (1213) using a mesoscale coupled WRF-ROMS model, *Ocean Eng.*, 175: 1-15.  
444 <https://doi.org/10.1016/j.oceaneng.2019.01.053>, 2019b.

445 Yeh, J. R., Shieh, J. S., and Huang, N. E.: Complementary ensemble empirical mode decomposition: A novel  
446 noise enhanced data analysis method, *Adv. Adap. Data Anal.*, 2, 135-156,  
447 <https://doi.org/10.1142/S1793536910000422>, 2010.

448 Zheng, X. T., Xie, S. P., Lv, L. H., and Zhou, Z. Q.: Intermodel uncertainty in ENSO amplitude change tied  
449 to Pacific Ocean warming pattern, *J. Climate*, 29, 7265-7279, <https://doi.org/10.1175/JCLI-D-16-0039.1>,  
450 2016.

451 Zhu, J., Huang, B., Kumar, A., and Kinter, J. L.: Seasonality in prediction skill and predictable pattern of  
452 tropical Indian Ocean SST, *J. Climate*, 28, 7962-7984, <https://doi.org/10.1175/JCLI-D-15-0067.1>, 2015.